Enhanced C3+alcohol synthesis from syngas using KCoMoSx catalysts

Xi, Xiaoying; Zeng, Feng; Cao, Huatang; Cannilla, Catia; Bisswanger, Timo; de Graaf, Sytze; Pei, Yutao; Frusteri, Francesco; Stampfer, Christoph; Palkovits, Regina

Published in:
Applied catalysis b-Environmental

DOI:
10.1016/j.apcatb.2020.118950

Publication date:
2020

Applied Catalysis B: Environmental 272 (2020) 118950

Contents lists available at ScienceDirect

Applied Catalysis B: Environmental

journal homepage: www.elsevier.com/locate/apcatb

Enhanced C3+ alcohol synthesis from syngas using $KCoMoS_x$ catalysts: effect of the Co-Mo ratio on catalyst performance

Xiaoying Xi[a,1], Feng Zeng[b,1], Huatang Cao[c], Catia Cannilla[d], Timo Bisswanger[e], Sytze de Graaf[f], Yutao Pei[c], Francesco Frusteri[d], Christoph Stampfer[e], Regina Palkovits[b,*], Hero Jan Heeres[a,*]

[a] Green Chemical Reaction Engineering, Engineering and Technology Institute Groningen, University of Groningen, Nijenborgh 4, 9747 AG Groningen, the Netherlands
[b] Chair of Heterogeneous Catalysis and Chemical Technology, ITMC, RWTH Aachen University, Worringerweg 2, 52074 Aachen, Germany
[c] Department of Advanced Production Engineering, Engineering and Technology Institute Groningen, University of Groningen, Nijenborgh 4, 9747AG, the Netherlands
[d] Institute of Advanced Technologies for Energy N. Giordano, Via S. Lucia sopra Contesse, n. 5, 98126 Messina, ME, Italy
[e] 2nd Institute of Physics A, RWTH Aachen University, 52074 Aachen, Germany
[f] Zernike Institute for Advanced Materials, University of Groningen, Nijenborgh 4, 9747 AG, Groningen, the Netherlands

A R T I C L E I N F O

Keywords:
Higher alcohols
syngas
Mo based catalysts

A B S T R A C T

K-Co-MoS_x catalysts varying in Co content were prepared to investigate the role of Co in this catalyst formulation for the synthesis of C3+ alcohols from syngas. The Co-MoS_x precursors and the best performing K-doped version were characterized in detail and the amount of active cobalt sulfide and mixed metal sulfide (Co-Mo-S) phases were shown to be a function of the Co content. The catalysts were tested in a continuous set-up at 360 °C, 8.7 MPa, a GHSV of 4500 mL g^{-1} h^{-1} and a H_2/CO ratio of 1. The highest alcohol selectivity of 47.1%, with 61% in the C3+ range, was obtained using the K-Co-MoS_x catalyst with a Co/(Co + Mo) molar ratio of 0.13. These findings were rationalized considering the amount and interactions between cobalt sulfide and Co-Mo-S or MoS_2 phases. Process studies followed by statistical modeling gave a C3+ alcohol selectivity of 31.0% (yield of 9.2%) at a CO conversion of 29.8% at optimized conditions.

1. Introduction

The depletion of fossil resources together with a strong drive to limit greenhouse gas emissions has led to an increasing effort in the development of sustainable and green transportation fuels. Well known examples are ethanol from sugars using fermentative approaches [1] and biodiesel from vegetable oils [2], which have both been commercialized in the last decades. When considering ethanol, some disadvantages have been identified, including a low energy density, high vapor pressure and high water solubility, which cause corrosion issues when using ethanol-rich ethanol-gasoline blends [3]. These disadvantages may be alleviated by using C3+ alcohols, which have superior fuel properties, such as higher energy density, lower volatility and better solubility in hydrocarbons (HC), while at the same time possessing comparable octane numbers as found for gasoline [4].

When considering chemo-catalytic routes to higher alcohols, syngas appears an interesting feed [5]. Various catalytic systems have been identified for this purpose [6]. Among them, molybdenum sulfide-based catalysts are of particular interest due to their low cost, high water-gas shift activity and high resistance to sulfur poisoning [7], thus avoiding the need for water separation and deep desulfurization units. MoS_2 alone mainly produces CO_2 and hydrocarbons (HC) from syngas, while alkali metals, especially potassium (K) modified MoS_2 catalysts are commonly used to achieve good selectivity for alcohols [8]. K promotion suppresses hydrogenation of metal-alkyl species to HCs and enhances the rate of CO insertion in the M-alkyl bond to form metal-acyl species, which are subsequently converted to alcohols [9]. It is proposed that $KMoS_2$ phases, formed by the intercalation of K into the MoS_2 structure, are responsible for the higher selectivity to alcohols when compared to MoS_2 alone [10–13].

However, K modified MoS_2 catalysts normally suffer from low activity [6], leading to relatively low CO conversion and thus a low yield of alcohols. Efforts have been undertaken on tailoring the structure of the K modified MoS_2 catalysts to enhance the selectivity to C3+ alcohols [14,15]. In previous work from our groups, we prepared multilayer K modified MoS_2 catalysts with well-contacted MoS_2 and $KMoS_2$ phases and showed that these catalysts lead to improved alcohol selectivities [16]. Another approach involves promotion by group VIII metals, such

* Corresponding authors.
E-mail addresses: palkovits@itmc.rwth-aachen.de (R. Palkovits), h.j.heeres@rug.nl (H.J. Heeres).
[1] These authors have contributed equally to this work.

https://doi.org/10.1016/j.apcatb.2020.118950
Received 11 October 2019; Received in revised form 21 March 2020; Accepted 28 March 2020
Available online 13 April 2020
0926-3373/

as Co and Ni [7,17–19]. Especially cobalt is known to promote carbon chain growth, leading to higher selectivities to higher alcohols [20,21], though often ethanol is the major product.

Co promoted MoS_2 catalysts are widely used in hydrodesulfurization (HDS) reactions and the promoting effect of Co is attributed to the formation of a Co-Mo-S phase [22], formed by partial substitution of Mo atoms at the edge of MoS_2 slabs by Co atoms [23]. This particular phase has also been observed in K modified, Co promoted MoS_2 catalysts for alcohol synthesis [18,20,24–27]. To elucidate the function of cobalt, Mo free, K modified cobalt sulfide catalysts were employed for the reaction. In this case, the amount of higher alcohols was low and C1-C4 alkanes were prevailing [20], indicating that K-CoS_x phases are not suitable for higher alcohol synthesis. It also has been shown that, the number of active Co-Mo-S species decreases at high Co loadings due to the formation of Co_9S_8 phases, which are stable under typical reaction conditions and have a low activity for higher alcohols [28–31].

Thus, literature data imply that a Co-Mo-S phase in Co promoted MoS_2 catalysts is the active phase, [20,28–33], though the exact mechanism to promote carbon chain growth is still under debate. However, the role of both K and Co in K modified $CoMoS_x$ catalysts has not been explored in detail. We therefore performed a systematic investigation on the effect of these promotors on the performance of MoS_2 catalysts for higher alcohol synthesis from syngas. For this purpose, a series of K modified Co promoted molybdenum sulfide catalysts with different Co contents and a fixed K content were prepared, characterized in detail and tested for the conversion of syngas to higher alcohols. The results were compared with a Mo free catalyst in the form of K-CoS_x and a K-free catalyst ($CoMo_x$-0.13). In addition, for the optimized catalyst regarding Co content, the effect of process conditions, such as temperature (T), pressure (P), gas hourly space velocity (GHSV) and H_2/CO ratio was explored. The results were quantified using statistical approaches allowing determination of the optimal process conditions for higher alcohol selectivity and yield.

2. Experimental Section

2.1. Catalyst preparation

The cobalt-molybdenum sulfide was prepared by sulfurization of the cobalt-molybdenum oxide precursor with KSCN according to a method reported in the literature [34] with some modifications. The cobalt-molybdenum oxide precursor was typically synthesized by mixing $Co(NO_3)_2{\cdot}6H_2O$ and $(NH_4)_6Mo_7O_{24}{\cdot}4H_2O$ (20 g in total, Sigma-Aldrich) in 50 mL of deionized water. The resulting suspension was heated and maintained at 120 °C for 3 h, during which most of the water evaporated. The resulting mixture was calcined in air at 500 °C for 3 h to form the cobalt-molybdenum oxide. The amount of $Co(NO_3)_2{\cdot}6H_2O$ and $(NH_4)_6Mo_7O_{24}{\cdot}4H_2O$ was varied to adjust the atomic ratio Co/(Co + Mo) between 0 and 0.7.

For sulfurization, the cobalt-molybdenum oxide (0.648 g), KSCN (0.875 g, Sigma-Aldrich), and deionized water (35 mL) were mixed in an autoclave, which was kept at 200 °C for 24 h. Then the autoclave was rapidly cooled with ice, and the resulting precipitate was filtered and washed with deionized water (total 500 mL). The product was obtained after drying at ambient conditions overnight. The molybdenum sulfide is labelled as MoS_x and the mixed metal sulfide catalysts are labelled as Co-MoS_x-*R*, where *R* represents the actual Co/(Co + Mo) ratio as obtained from ICP-OES. The elemental composition of the sulfurized catalysts is shown in Table 1.

The K promoted K-Co-MoS_x-0.13 catalyst, used for detailed analyses by XRD, HRTEM and STEM with EDS mapping, was prepared by physically mixing Co-MoS_x-0.13 with K_2CO_3 followed by a treatment under hydrogen (1 bar, 8 h, 400 °C) and subsequent passivation (1% O_2/N_2, 4 h, 25 °C).

The K promoted CoS_2 catalyst was prepared by physically mixing a CoS_2 sample (Sigma Aldrich) with K_2CO_3 followed by a reduction procedure as described above.

Table 1
Physical and chemical properties of the sulfurized catalysts.

Catalyst	$R_{Co/(Co+Mo)}$ [a]	S_{BET} [b] ($m^2\ g^{-1}$)	V_{sgp} [c] ($cm^3\ g^{-1}$)	D_{BJH} [d] (Å)
MoS_x	0	9.7	0.05	155
Co-MoS_x-0.13	0.13	11.5	0.07	184
Co-MoS_x-0.37	0.37	8.2	0.04	163
Co-MoS_x-0.53	0.53	7.2	0.03	164
Co-MoS_x-0.63	0.63	7.7	0.03	158

[a] Mole ratio of cobalt to cobalt and molybdenum as determined experimentally.
[b] Specific surface area by the BET method.
[c] Single point pore volume.
[d] Pore diameter by BJH method.

2.2. Catalyst characterization

The cobalt-molybdenum sulfide samples were characterized with ICP-OES (Spectroblue, Germany) to quantify the elemental composition.

The specific surface area and pore parameter were determined using N_2 physisorption, which was conducted at 77 K using an ASAP 2420 system (Micromeritics, USA). Prior to analysis, the samples were degassed at 150 °C under vacuum for 12 h. The specific surface area was calculated using the Brunauer-Emmett-Teller (BET) method in the P/P_0 range of 0.05–0.25. The total pore volume was estimated from the single point desorption data at P/P_o = 0.97. The pore diameter was obtained from the desorption branch according to the Barrett-Joyner-Halenda (BJH) method.

X-ray diffraction (XRD) patterns of the sulfurized samples were collected for a 2θ scan range of 5–80° on a D8 Advance powder diffractometer (Bruker, Germany) with CuKα radiation (λ = 1.5418 Å) operated at 40 kV and 40 mA. XRD spectra of the K modified sample (K-Co-MoS_x-0.13) were recorded in the same way.

H_2-TPR measurements were conducted using 10 vol.% H_2 in He (30 ml min^{-1}) and the samples were heated from room temperature to 900 °C at a temperature ramp of 10 °C/min using an AutoChem system (Micromeritics, USA) equipped with a thermal conductivity detector (TCD). Raman spectroscopy was measured using a WITec Alpha 300R microscope with a 532 nm excitation laser.

The micro-structure of the sulfurized samples was examined with high-resolution transmission electron microscopy (HRTEM, JEOL 2010 FEG, Japan) operating at 200 kV. The samples were first ultrasonically dispersed in ethanol and then deposited on a carbon-coated copper grid. Processing of the HRTEM images was accomplished using DigitalMicrograph software.

High-angle annular dark-field scanning transmission electron microscopy (HAADF-STEM) images of the K-Co-MoS_x-0.13 sample were obtained using a probe and image aberration corrected Themis Z microscope (Thermo Fisher Scientific) operating at 300 kV in STEM mode with a convergence semi-angle of 21 mrad and a probe current of 50 pA. Energy dispersive X-ray spectroscopy (EDS mapping) results were achieved with a Dual X EDS system (Bruker) with a probe current of 250 pA. Data acquisition and analysis were done using Velox software (version 2.8.0).

2.3. Catalytic testing in a continuous fixed-bed reactor

Reactions were performed in a continuous fixed-bed reactor (stainless steel) with an internal diameter of 10 mm. Typically, the cobalt-molybdenum sulfide catalyst (0.35 g) was physically mixed with K_2CO_3 (0.05 g, Sigma-Aldrich) and SiC (2.0 g, Sigma-Aldrich) and then loaded to the reactor. Before reaction, the catalyst was reduced *in situ* using a flow of H_2 (50 ml min^{-1}) at 400 °C for 8 h. After cooling to room temperature under a N_2 stream, the reaction was started by switching to a gas mixture of H_2/CO (molar ratio ranging from 1.0 to 2.0) with 6%

N_2 (internal standard). Typical reaction conditions are pressures between 8.7 and 14.7 MPa and temperatures between 340 and 380 °C. The gas hourly space velocity (GHSV) was varied from 4500 to 27000 mL g^{-1} h^{-1} by adjusting the flow rate of the feed gas. The reactor effluent was cooled and the liquid product was separated from the gas phase by using a double walled condenser at −5 °C. Details regarding product analysis are described in a previous publication from our groups [16]. The CO conversion (X_{CO}), the product selectivity (S_i) and yield (Y_i) were calculated using Eqs. (1)–(3).

$$X_{CO} = \frac{moles\ of\ CO_{influent} - moles\ of\ CO_{effluent}}{moles\ of\ CO_{influent}} \times 100\% \quad (1)$$

$$S_i = \frac{moles\ of\ product\ i \times number\ of\ carbons\ in\ product\ i}{moles\ of\ CO_{influent} - moles\ of\ CO_{effluent}} \times 100\% \quad (2)$$

$$Y = X_{CO} \times S_i \quad (3)$$

The activity data given in this study are the average for at least 6 h runtime and collected after 20 h, to ensure stable operation of the reactor. The selectivity of all products is carbon based and only data with carbon balances higher than 95% are reported here.

The chain growth probability α was determined from the experimental data assuming an ASF distribution for the alcohols (Eq. (4)).

$$\frac{S_n}{n} = \alpha^n \times \frac{(1-\alpha)}{a} \quad (4)$$

Here, S_n is the selectivity of the alcohols with a carbon number of n, n is the carbon number, and α is the chain growth probability. The value of α was determined by plotting $ln(\frac{S_n}{n})$ against n.

2.4. Statistical modeling

Multivariable regression was used to quantify the effect of process conditions (T, P, GHSV and H_2/CO ratio) on catalytic performance (Eq. (5)).

$$Y = a_0 + \sum a_i x_i + \sum a_{ii} x_i^2 + \sum a_{ij} x_i x_j \quad (5)$$

Here x is independent variable (T, P, GHSV and H_2/CO ratio) and Y is a dependent variable (selectivity and yield of C3+ alcohol), a_i, a_{ii}, and a_{ij} are the regression coefficients and a_0 is the intercept. The regression coefficients were determined using the Design-Expert (Version 7) software by backward elimination of statistically non-significant parameters. The significant factors were selected based on their *p*-value in the analysis of variance (ANOVA). A parameter with a *p*-value less than 0.05 is considered significant and is included in the response model.

3. Results and discussion

3.1. Characterization of the cobalt-molybdenum sulfide catalysts

The cobalt-molybdenum sulfide catalysts with different Co contents were prepared by sulfurization of the corresponding cobalt-molybdenum oxide precursors using KSCN. The actual Co/(Co + Mo) molar ratio was determined by ICP-OES and ranged from 0 to 0.63 (Table 1). The textural properties of the sulfurized catalysts (without K addition) are depending on the Co content, see Table 1 for details. When considering the specific surface area, a maximum was found for Co-MoS_x-0.13, with a value of 11.5 m^2 g^{-1}. This value is in the broad range reported in the literature for Co-MoS_x catalysts (from single digit values to several hundred square meters per gram [35]), rationalized by differences in the Co and Mo precursors used and synthesis conditions. The observed reduction at higher Co amounts may be due to the formation of a segregated Co sulfide phase [36]. Similar trends were observed for the pore volume and pore diameters of the catalysts, *viz*. the highest value was found for catalyst Co-MoS_x-0.13.

The XRD patterns of the catalyst (without K addition) are shown in Fig. 1. The MoS_x catalyst shows broad diffractions at 2θ values of about 14°, 33°, 36° and 58°, which are associated with the (0 0 2), (1 0 0), (1 0 2) and (1 1 0) planes, respectively, of the 2H-MoS_2 phase (JCPDS card No. 00-037-1492). Upon the addition of Co, the reflexes of the crystalline MoS_2 phase disappear and new signals arise. These were identified as cobalt-containing species like CoS_2 (JCPDS card No. 01-089-3056), $CoMoS_{3.13}$ (JCPDS card No. 00-016-0439) and $CoMoO_4$ (JCPDS card No. 00-021-0868). Of interest is the presence the $CoMoS_{3.13}$ phase, which is known to be formed by partial substitution of Mo atoms at the edges of MoS_2 sheets by Co. Mixed Co-Mo-S phases are generally thought to be active for higher alcohol synthesis by promoting carbon chain growth [6]. At high Co loadings, sharp reflexes from crystalline CoS_2 and $CoMoO_4$ are present, suggesting a higher abundance and larger nanoparticle sizes. Reflexes attributed to a Co_9S_8 phase, reported to be present at higher Co loadings, were not detected [30].

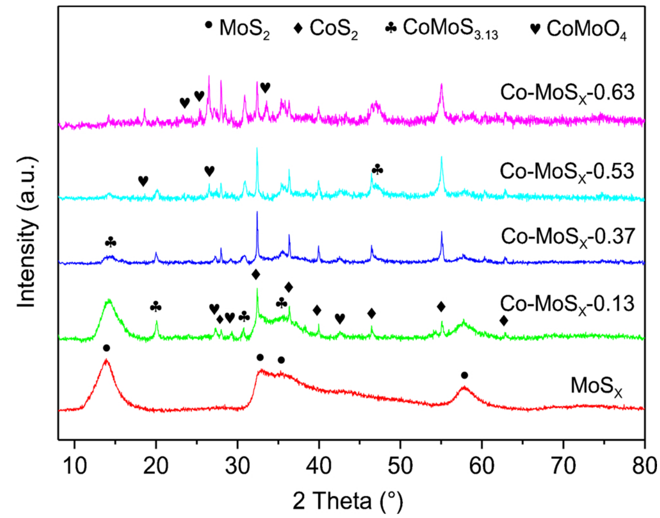

Fig. 1. XRD patterns of the cobalt-molybdenum sulfide catalysts with different Co/(Co + Mo) molar ratios.

H_2-TPR measurements were performed for all sulfided Co-Mo catalysts and the profiles are given in Fig. 2. The Co free MoS_x catalyst displays two H_2 peaks, a small one at 310 °C and a larger one at about 720 °C. The first peak is ascribed either to the presence of over-stoichiometric S_x species or to weakly bonded sulfur anions along MoS_2 edges [37]. The high temperature peak is associated with more strongly bound sulfur anions located at the edges [38]. Another possibility is a

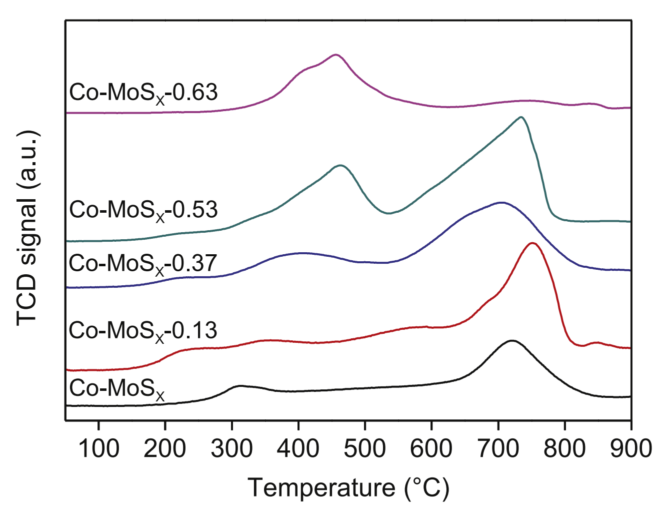

Fig. 2. H_2-TPR profiles of the cobalt-molybdenum sulfide catalysts with different Co/(Co + Mo) molar ratios.

phase formed by desulfurization of the MoS_2 phase by elimination of basal sulfur, though not likely as temperatures higher than 830–1030 °C are required for this transition [39]. Upon the addition of Co, additional peaks become visible. The low temperature peak is shifted to lower temperatures (about 220 °C), indicating that the presence of Co leads to a weakening of the Mo-S bond [40]. A similar low temperature peak was also observed during H_2-TPR measurements on supported Co-MoS_2/Al_2O_3 catalysts for HDS reactions and associated with the presence of a Co-Mo-S phase [41]. The area of the first peak is reduced when adding more Co in the catalyst formulation. Besides, a new peak at an intermediate temperature (370–470 °C) appears, which is ascribed to a cobalt sulfide phase [41]. In line with this explanation is the observation that the area of this particular peak increases with increasing Co content. This suggests that for low Co/(Co + Mo) ratios, the Co atoms are dispersed at the edge of a MoS_2 phase to form a Co-Mo-S phase, whereas higher Co amounts lead to the formation of Co sulfide species. These may be present as a single phase or closely interact with Co-Mo-S and MoS_2 phases.

The Raman spectra of the sulfided Co-Mo catalysts (without K) are shown in Fig. 3. The unpromoted MoS_x catalyst exhibits two peaks at 380 cm^{-1} and 405 cm^{-1}, which are ascribed to the in-plane E^1_{2g} and out-of-plane A_{1g} vibration mode of the MoS_2 layer structure [42]. These two bands are also detected in Co-MoS_x-0.13, and the distance between the two bands, which is an indicator for the interlayer distance between the MoS_2 stacked layers [15,43], is similar to that for the unpromoted MoS_x catalyst. This suggests that, different with K [12], Co is not intercalated in the interlayer space of MoS_2 phase, which is consistent with the H_2-TPR result. For the catalysts with high Co contents, the two peaks disappear, and a new peak at 931 cm^{-1} emerges, associated with the formation of a β-$CoMoO_4$ phase, which is in consistent with the XRD results. The intensity of the peak increases with increasing Co content.

HRTEM was used to determine the morphology and microstructure of the catalysts. Representative images are displayed in Fig. 4. The MoS_x catalyst without Co shows a multilayer structure with a lattice spacing of 0.63 nm, corresponding to the (0 0 2) plane of the MoS_2 phase (Fig. 4a) [44]. After the addition of Co, various Co-containing species were identified based on their specific lattice fringes. Examples are Co-MoS_x, CoS_x and $CoMoO_4$ phases (Fig. 4b–f). The lattice fringe with a lattice spacing of 0.25 nm corresponds to the (2 1 0) plane of CoS_2.

Of interest is the observation of close contacts between the CoS_2 and MoS_2 phase for Co-MoS_x-0.13 (Fig. 4b–c), indicating the presence of a CoS_2/MoS_2 interface. The presence of this interface has been reported to be beneficial for higher alcohol formation [45]. The phase with a lattice spacing of 0.63 nm may be either from MoS_x or a $CoMoS_{3.13}$ species. For catalysts with a higher Co content (e.g. Co-MoS_x-0.37), a $CoMoO_4$ phase is present (lattice fringe with a spacing of 0.68 nm (Fig. 4d)), consistent with the XRD analysis.

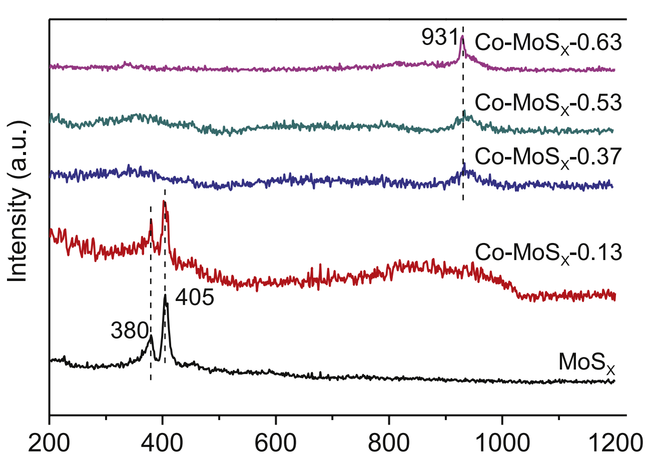

Fig. 3. Raman spectra of the cobalt-molybdenum sulfide catalysts with different Co/(Co + Mo) molar ratios.

With the catalyst characterization data available, the effect of the amount of Co on catalyst structure may be assessed. Unpromoted MoS_x reveals a multilayer structure with long-range ordered MoS_2 domains, in line with the literature data. After promotion with Co, Co-Mo-S and CoS_2 phases are formed, which are considered possible active phases for higher alcohol synthesis (Co-MoS_x-0.13). At higher Co contents, higher amounts of CoS_2 and $CoMoO_4$ species are present, which may have a negative effect on catalyst performance (*vide infra*).

Finally, the K promoted version of Co-MoS_x-0.13 (K-Co-MoS_x-0.13), which is the best catalyst in terms of performance for higher alcohol synthesis (*vide infra*), was characterized in detail using XRD, HRTEM and STEM with EDS mapping to gain insights in changes in the structure upon the addition of K. The sample was prepared by physically mixing Co-MoS_x-0.13 with K_2CO_3 followed by reduction with hydrogen and passivation (see experimental section).

XRD spectra of K-Co-MoS_x-0.13, together with MoS_x and Co-MoS_x-0.13 for comparison, are given in Fig. 5a. The (002) reflex of K-Co-MoS_x-0.13 at 13.3° is slightly shifted downfield compared to that of MoS_2 (14.1°), indicating an expanded interlayer spacing due to the incorporation of K. A HRTEM image (Fig. 5b) of K-Co-MoS_x-0.13 confirms the expanded interlayer spacing (0.77- 0.81 nm *vs* 0.63 nm for Co-MoS_x-0.13, Fig. 4c) after K addition. The intercalation of K into the MoS_2 structure leads to the formation of a $KMoS_2$ phase, which was discussed in detail in our previous work [16] and is suggested to be essential for alcohol synthesis.

The reflexes of CoS_2, clearly visible in Co-MoS_x-0.13, are absent in the XRD spectrum of K-Co-MoS_x-0.13. New reflexes at 30.1°, 31.2° and 39.7°, identified as Co_9S_8 species (JCPDS card No. 00-003-0631) are present. The Co_9S_8 species are likely formed by reduction of CoS_2, which is consistent with the H_2-TPR results (Fig. 2). Representative reflexes of crystalline $CoMoS_{3.13}$ are also present in K-Co-MoS_x-0.13. The presence of both Co_9S_8 and $CoMoS_{3.13}$ species in K-Co-MoS_x-0.13 is confirmed by HRTEM images (Fig. 5c–d). Close contacts between the Co_9S_8 and K promoted (Co)MoS_x phase were observed (Fig. 5b–d), in agreement with the observation of CoS_2/(Co)MoS_x interfaces in the unpromoted Co-MoS_x-0.13 catalyst (Fig. 4b–c).

A STEM dark field image combined with EDS mapping (Fig. S1) of K-Co-MoS_x-0.13 shows that K, Co, Mo and S are uniformly dispersed in the catalyst. Such a homogeneous distribution is indicative for the presence of abundant Co_9S_8/K-(Co)MoS_x interfaces in K-Co-MoS_x-0.13.

3.2. Higher alcohol synthesis using K promoted Co-MoS_x catalysts with different Co contents

Benchmark experiments with all catalysts were performed at 360 °C, 8.7 MPa, a GHSV of 4500 mL g^{-1} h^{-1} and a H_2/CO ratio of 1 in a continuous packed bed reactor set-up. These conditions were selected based on previous experience in our group on the use of MoS_2 catalysts for higher alcohol synthesis [16]. Prior to reaction, the catalysts were promoted with K using a physical mixing method followed by an *in situ* treatment with H_2. The same amount of K was used for all catalyst formulations. The experiments were performed for at least 6 h and the performance of the catalyst was the average over the time period from 20 h to final runtime and thus taken at steady state conditions in the reactor (Table 2).

A typical example of the product selectivity and CO conversion versus the runtime is given in Fig. 6 (340 °C, 11.7 MPa, GHSV of 4500 mL g^{-1} h^{-1} and H_2/CO ratio of 1.5 using the K-Co-MoS_x-0.13 catalyst). It also shows the catalyst is stable for at least 100 h without co-feeding of sulfur.

Typical reactions products are alcohols (methanol, ethanol, and C3+ alcohol), hydrocarbons (methane and higher ones) and CO_2. The latter is formed by the water-gas shift reaction involving CO and water. The unpromoted K-MoS_x catalyst provides a selectivity of 40.8% to alcohols and 24.8% to hydrocarbons at a CO conversion level of 25.6%

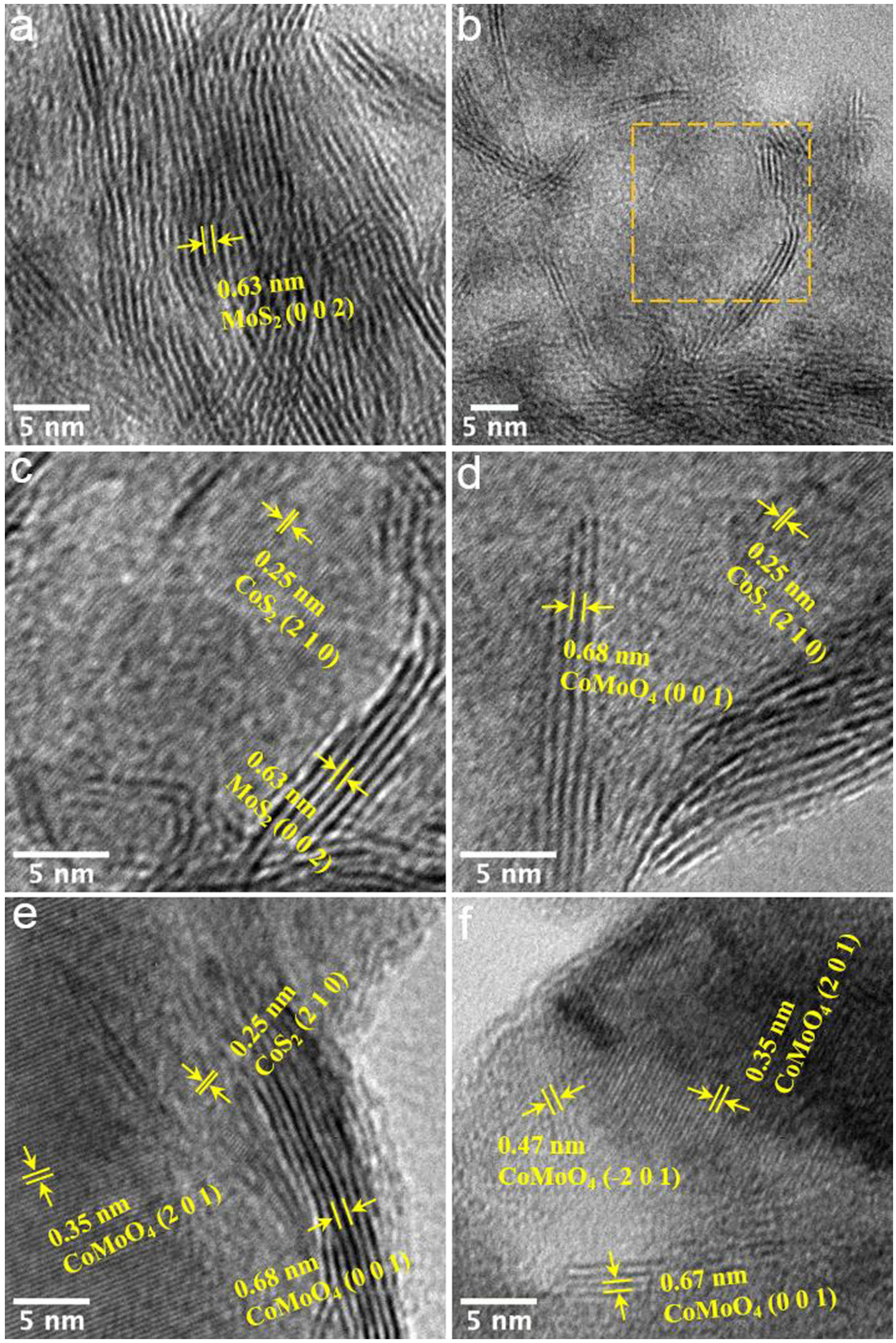

Fig. 4. HRTEM images of MoS_x (a), Co-MoS_x-0.13 (b-c), Co-MoS_x-0.37 (d), Co-MoS_x-0.53 (e) and Co-MoS_x-0.63 (f). (c) is the close-view of the marked area in (b).

(Fig. 7), which is typical for Mo-based catalysts [6]. Upon the addition of Co to the catalyst formulation, the CO conversion decreases, which may be due to the reduced availability of the active sulfided Mo-Co species by coverage with inactive $CoMoO_4$ species and/or the presence of less active CoS_2 species, as observed from XRD and HRTEM results.

The selectivity is a clear function of the Co content. Alcohol selectivity reaches a maximum (47.1%) for the K-Co-MoS_x-0.13 catalyst and decreases with higher Co loadings, see Fig. 7 for details. The selectivity to hydrocarbons (mainly CH_4), shows a reverse trend, whereas the CO_2 selectivity is about constant. The product selectivity at two other temperatures (340 and 380 °C) also shows a similar trend regarding the Co content in the catalyst formulation (Table S2).

The effect of Co addition on the carbon distribution of the alcohols is given in Fig. 8a. It shows that the amount of C3+ alcohols reaches a maximum at 59.0% for the K-Co-MoS_x-0.13 catalyst and decreases at higher Co amounts. The individual distribution of alcohols for the unpromoted K-MoS_x, K-Co-MoS_x-0.13 and K-Co-MoS_x-0.63 catalyst are depicted in Fig. 8b (the distributions for other catalysts are shown in Fig. S2) as Anderson-Schulz-Flory (ASF) plots. The unpromoted K-MoS_x catalyst shows a large deviation for particularly methanol when considering an ideal linear ASF distribution. This is in line with previous findings of our group, rationalized by assuming an enhanced chain growth mechanism for C3+ alcohol using these types of catalysts [16]. After loading with Co, an even larger deviation for methanol and also for ethanol is observed for the K-Co-MoS_x-0.13 catalyst. However, the deviation is less pronounced when further increasing the Co content

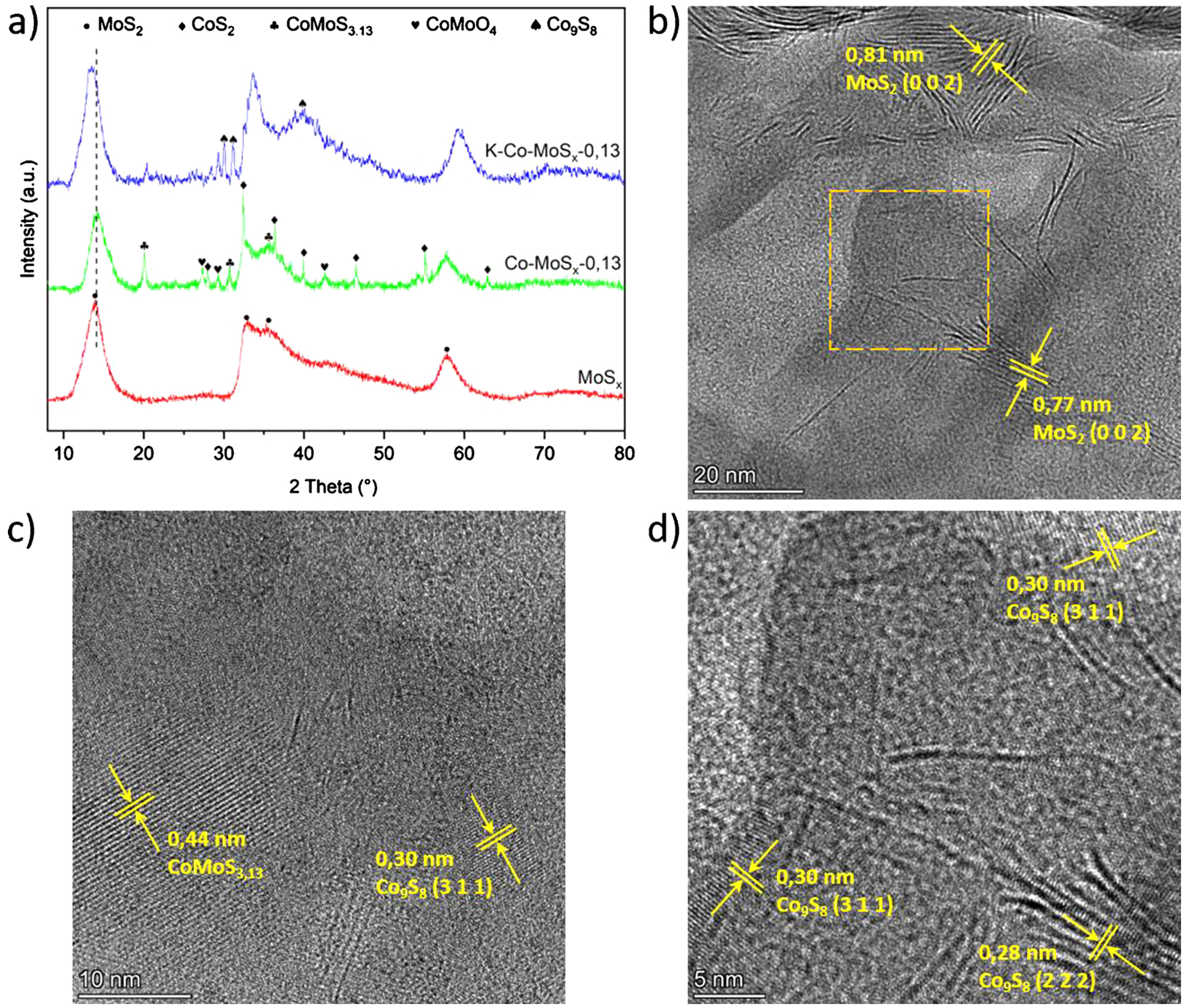

Fig. 5. a) XRD patterns of MoS_x, $CoMoS_x$-0.13 and K-$CoMoS_x$-0.13 catalyst. b-c) HRTEM images of K-Co-MoS_x-0.13. d) is the close-view of the marked area in b).

(Fig. S2) and the K-Co-MoS_x-0.63 catalyst shows an almost perfect linear distribution for the mixed alcohols including methanol. The carbon chain growth probability was calculated for the C2+ alcohols, showing a volcano-shaped curve with a peak for the K-Co-MoS_x-0.13 catalyst (Fig. S3). Thus, alcohol selectivity and carbon chain growth are best for the K-Co-MoS_x-0.13 catalyst, whereas higher Co contents lead to a higher hydrocarbon selectivity and a lower carbon chain growth for the alcohols.

For comparison, and also to determine the role of Mo in the catalyst formulation, the catalytic performance of a K promoted CoS_2 catalyst was also investigated. We first attempted to prepare the CoS_2 catalyst by a similar procedure as used for the Co-MoS_x samples (viz. sulfurization of the cobalt-oxide precursors using KSCN). However, Co_3O_4 instead of CoS_2 was obtained (Fig. S4), indicating that Co-oxides are difficult to sulfurize using KSCN at the prevailing conditions. Therefore, CoS_2 (Sigma-Aldrich) was used as the catalyst precursor, and after K addition and pretreatment (*in situ* reduction with H_2 at 400 °C for 8 h) tested for higher alcohol synthesis (360 °C, 8.7 MPa, GHSV of 4500 mL g^{-1} h^{-1} and H_2/CO molar ratio of 1). A very high hydrocarbon selectivity of 63.1% was achieved at a CO conversion of 1.3% (Table S3). Higher alcohols could not be detected in the liquid phase. The low CO conversion might be due to the presence of large crystallites (76 nm, from

Table 2
Catalytic performance of K-MoS_x and K-Co-MoS_x catalysts for the conversion of syngas to mixed alcohols.[a]

Catalyst	X_{CO}[b] (%)	Selectivity (%)					Alcohol distribution (%)		
		CH_4	HC[c]	CO_2	Alcohols	Others[d]	Methanol	Ethanol	C3+OH[e]
K-MoS_x	25.6	17.7	24.8	31.8	40.8	2.6	19.3	32.3	42.5
K-Co-MoS_x-0.13	18.7	16.8	19.9	29.5	47.1	3.5	11.3	26.9	54.9
K-Co-MoS_x-0.37	17.4	19.0	21.6	29.1	47.0	2.3	17.3	38.4	39.6
K-Co-MoS_x-0.53	12.3	19.1	22.1	28.4	46.0	3.5	22.7	41.6	28.6
K-Co-MoS_x-0.63	8.8	22.2	25.9	32.0	41.5	0.6	33.6	42.6	22.4

[a] Reaction conditions: 360 °C, 8.7 MPa, GHSV = 4500 mL g^{-1} h^{-1}, H_2/CO = 1.
[b] CO conversion.
[c] Hydrocarbons.
[d] Other liquid oxygenates except alcohols; [e] C3+ alcohol.

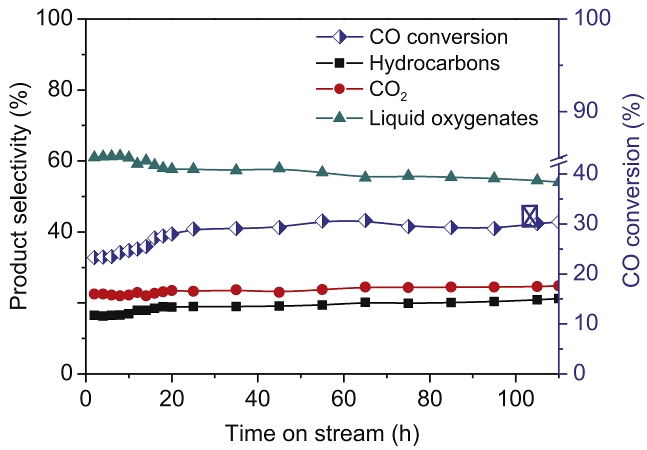

Fig. 6. Representative graph for CO conversion and product selectivity versus time on stream for the K-Co-MoS_x-0.13 catalyst. Reaction conditions: 340 °C, 11.7 MPa, GHSV = 4500 mL g^{-1} h^{-1}, H_2/CO = 1.5.

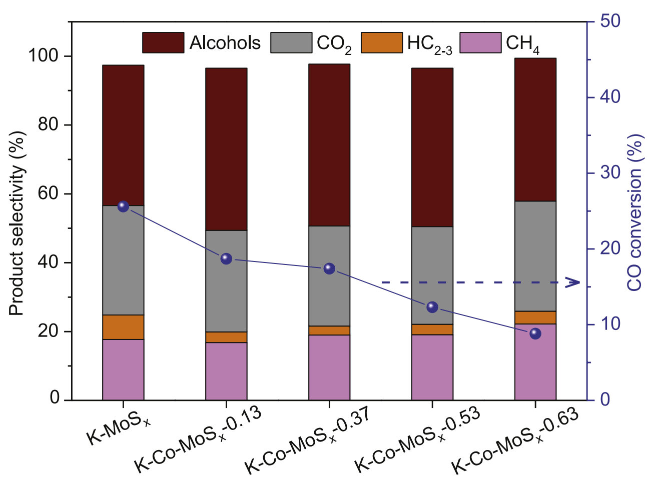

Fig. 7. CO conversion and product selectivity for catalysts with different Co contents. Reaction conditions: 360 °C, 8.7 MPa, GHSV = 4500 mL g^{-1} h^{-1}, H_2/CO = 1.

XRD data using Scherrer equation) and the lack of structural defects (Fig. S5). These findings are in line with experiments by Li et al., who reported that only C1-C4 alkanes and no alcohols were formed when using a K-CoS_x on activated carbon catalyst (in which Co is present in the form of Co_9S_8 crystallites) [20]. Co_9S_8 species, formed by reduction of CoS_2 were indeed detected after reaction (Fig. S5), in line with literature data [20].

3.3. Mechanistic implications

The unpromoted Co-MoS_x-0.13 catalyst (without K) showed high CO conversion and very low selectivity for alcohols (< 2%) in comparison with that of K-Co-MoS_x-0.13 (Table S4), indicating the important role of K for alcohol synthesis. Specifically, the presence of a $KMoS_2$ phase (Fig. 5) is considered to be essential for alcohol synthesis, see also previous work from our group [16]. This is also in agreement with literature data revealing that the addition of K in MoS_2 catalysts leads to lower hydrogenation rates while maintaining good CO insertion rates [8,9,46]. The obtained higher alcohols over the K modified catalyst are mainly composed of linear primary alcohols as well as branched alcohols like 2-methyl-1-propanol, 2-methyl-1-butanol, and 2-methyl-1-pentanol (Figs. S6–9). These branched alcohols were suggested to be formed via a β-addition process [47,48]. We have recently proposed that the linear primary alcohols are formed through CO insertion, while the branched alcohols are formed by CO insertion and CH_x β-addition [16,49], see Schema 1 for details. n-Propanol is formed through both routes, supported by the high amount (> 97%) of n-propanol in total propanol fraction (Fig. S6) (Scheme 1).

In the current investigation, the role of Co on product selectivity was investigated. Upon Co addition, the CH_4 selectivity is lowered slightly from 17.7% for K-MoS_x to 16.8% for the K-Co-MoS_x-0.13 catalyst. A further increase in Co in the catalyst formulation leads to a gradual increase in CH_4 selectivity (Fig. 7), suggesting a somewhat higher hydrogenation ability. The latter may be due to the presence of higher amounts of (K promoted) CoS_2 species (Figs. 1, 2 and 4) in the catalysts at higher Co contents.

The selectivity to alcohols in general and C3+ alcohols in particular shows an optimum for the K-Co-MoS_x-0.13 catalyst and decreases with higher Co loadings (Figs. 7 and 9). These findings are rationalized by considering that the amounts of Co-Mo-S and CoS_2 phases in the Co-MoS_x-0.13 catalyst are highest and that these are preferred for higher alcohol synthesis. At higher Co contents, considerable amounts of $CoMoO_4$ species are present which result in lower higher alcohol selectivity.

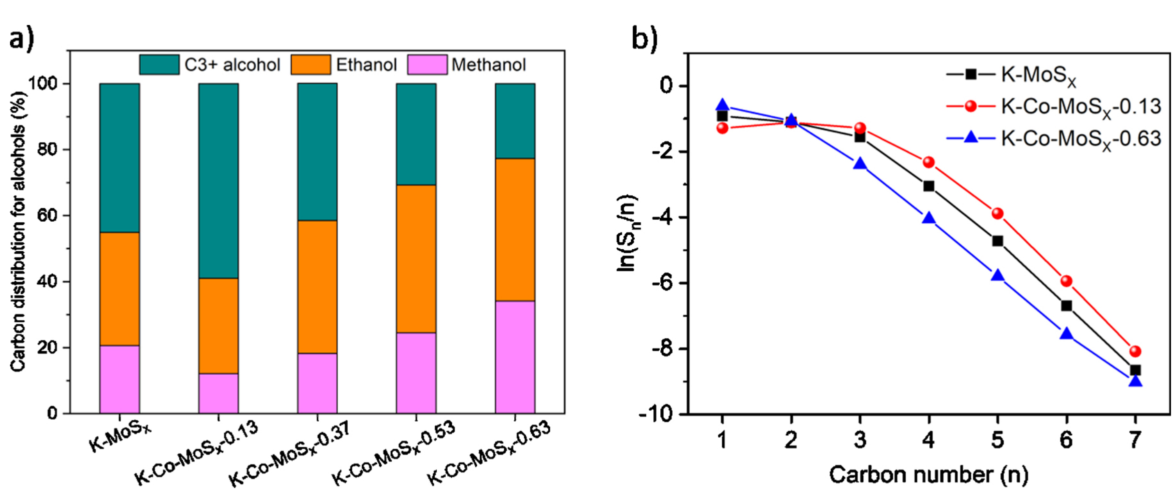

Fig. 8. a) Carbon distribution for the alcohols using catalyst with different Co contents. b) ASF plots for product alcohols using K-MoS_x, K-CoMoS_x-0.13 and K-CoMoS_x-0.63 catalysts. Reaction conditions: 360 °C, 8.7 MPa, GHSV = 4500 mL g^{-1} h^{-1}, H_2/CO = 1.

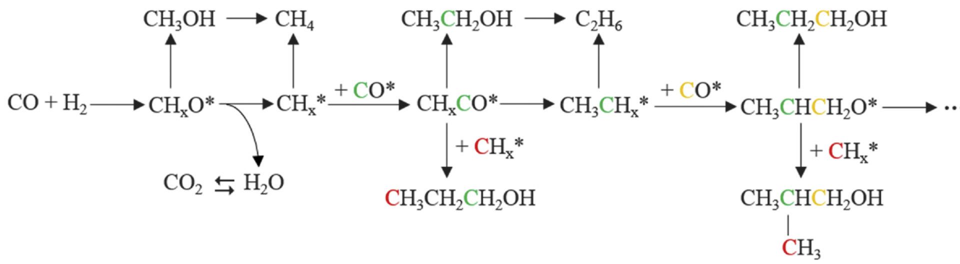

Scheme 1. Overall reaction network of syngas conversion over K modified MoS_2 catalyst.

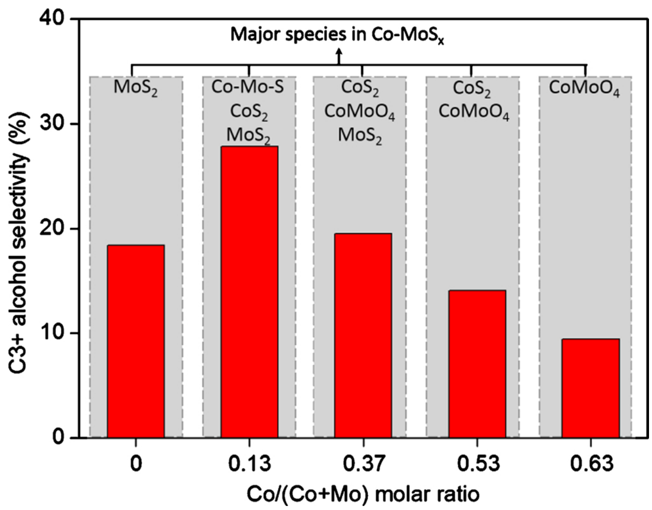

Fig. 9. C3+ alcohol selectivity for K-Co-MoS_x catalysts with different Co contents and major species in the corresponding Co-MoS_x samples. Reaction conditions: 360 °C, 8.7 MPa, GHSV = 4500 mL g^{-1} h^{-1}, H_2/CO = 1.

The trend as given in Fig. 9 holds for the unpromoted (no K) catalysts. Analyses of a K-promoted catalyst (K-Co-MoS_x-0.13) by XRD and HRTEM shows that the CoS_2 phase, is reduced to Co_9S_8 (Fig. 5). Based on these findings, we propose that the catalytic performance of the K-MoS_x catalyst is enhanced by the addition of Co due to the formation of cobalt sulfides (mainly Co_9S_8) and a K-promoted (Co)MoS_x phase in close proximity. This assembly is given in Scheme 2 and shows a (K promoted) Co_9S_8 phase sandwiched between two K-promoted (Co)MoS_x phases. The (K-)Co_9S_8 phase gives mainly hydrocarbons for syngas conversions, see results for the Mo free K-Co_x provided in this manuscript and literature data [20]. This implies the presence of significant amounts of adsorbed CH_x* (and higher carbon number analogs) on the surface of the Co_9S_8 phase. We assume that efficient transfer of such CH_x* species from the Co_9S_8 phase to adsorbed CH_3CHCH_2O* species on the K-(Co)MoS_x phase occurs, leading to branched alcohols (CH_x β-addition mechanism). In addition, linear alcohols are formed by transfer of adsorbed $CH_3CH_2CH_2$* on the Co_9S_8 phase to adsorbed CO on the K-(Co)MoS_x phase.

3.4. Statistical modeling of process variables on alcohol selectivity using the best catalyst in this study (K-Co-MoS_x-0.13)

To determine the effects of process conditions on CO conversion and product selectivity (particularly C3+ alcohols), a total of 44 experiments were performed in the continuous set-up at a range of 340–380 °C 8.7–14.7 MPa, GHSV of 4500–27000 mL g^{-1} h^{-1} and H_2/CO ratio of 1.0–2.0 for the best catalyst (K-Co-MoS_x-0.13) based on the benchmark experiments. In the initial stage, one variable was changed within the range while the other variables were kept constant (Figs. S10–18). This allows for determination of the individual effects of a variable on the CO conversion and product selectivity. In a later stage all experimental data (Table 3) were used simultaneously to develop multivariable nonlinear regression models of the form given in Eq. (5).

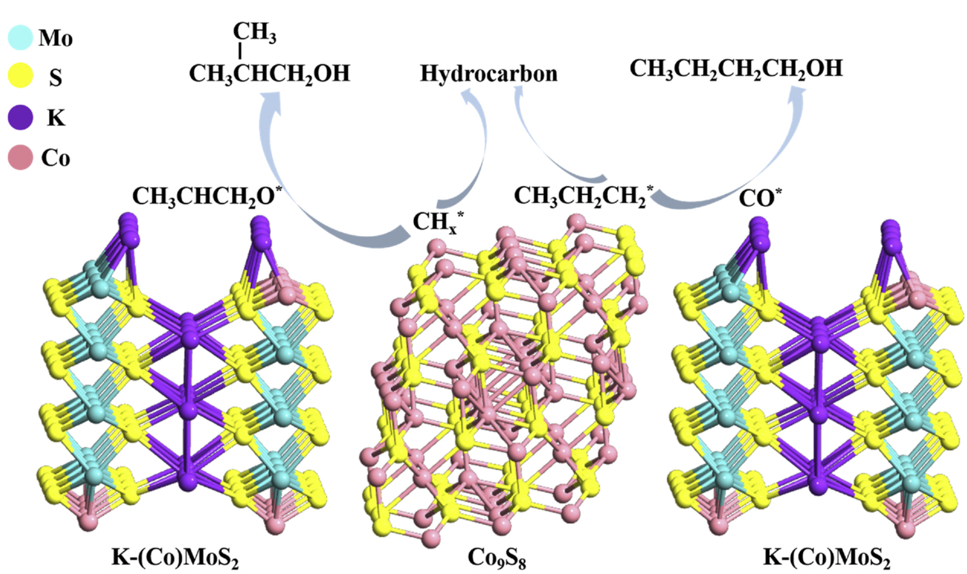

Scheme 2. Proposed syngas conversion network over K-Co-MoS_x catalyst.

Table 3
Overview of experiments for syngas conversions over the K-Co-MoS_x-0.13 catalyst.

Run	Pressure (MPa)	Temperature (°C)	GHSV (mL g^{-1} h^{-1})	H_2/CO ratio	C3+ alcohol yield (%)	C3+ alcohol selectivity (%)
1	8.7	340	4500	1	2.9	25.1
2	8.7	360	4500	1	5.2	27.8
3	8.7	380	4500	1	7.3	27.2
4	11.7	340	4500	1	2.1	8.6
5	11.7	340	9000	1	2.4	14.0
6	11.7	360	4500	1	6.5	16.8
7	11.7	360	9000	1	7.4	24.9
8	11.7	360	18000	1	5.5	29.3
9	11.7	360	27000	1	4.7	31.2
10	11.7	380	4500	1	8.2	17.7
11	11.7	380	13500	1	9.2	31.0
12	11.7	380	27000	1	7.3	37.6
13	14.7	340	4500	1	2.1	8.0
14	14.7	340	9000	1	2.5	13.6
15	14.7	340	13500	1	1.4	10.4
16	14.7	340	18000	1	1.5	13.6
17	14.7	360	4500	1	4.3	10.6
18	14.7	360	9000	1	5.4	16.9
19	14.7	360	18000	1	3.6	17.6
20	14.7	360	27000	1	2.2	15.2
21	14.7	380	4500	1	6.3	12.8
22	14.7	380	13500	1	7.2	22.2
23	14.7	380	27000	1	3.9	19.9
24	14.7	380	40500	1	2.6	18.5
25	11.7	340	4500	2	1.7	5.2
26	11.7	340	13500	2	1.6	9.8
27	11.7	340	18000	2	1.1	8.0
28	11.7	360	4500	2	4.2	9.1
29	11.7	360	13500	2	5.4	18.4
30	11.7	360	27000	2	3.9	20.6
31	11.7	380	4500	2	6.6	12.9
32	11.7	380	13500	2	8.3	23.4
33	11.7	380	27000	2	6.1	24.9
34	11.7	380	40500	2	4.4	22.8
35	11.7	340	4500	1.5	2.5	8.2
36	11.7	340	13500	1.5	3.0	18.9
37	11.7	340	27000	1.5	2.1	26.5
38	11.7	360	4500	1.5	4.5	11.1
39	11.7	360	9000	1.5	6.2	19.2
40	11.7	360	18000	1.5	5.3	24.5
41	11.7	360	27000	1.5	3.8	23.0
42	11.7	380	4500	1.5	6.6	13.4
43	11.7	380	13500	1.5	7.7	23.7
44	11.7	380	27000	1.5	6.4	29.2

This approach allowed the identification of interactions between the variables (T, P, GHSV and H_2/CO ratio) on the selectivity and yield of C3+ alcohol.

The yield (%) and selectivity (%) of C3+ alcohol as a function of reaction conditions were successfully modeled and the results are given in Eqs. (6) and (7), respectively.

$$Yield = 2.05 \times P + 0.13 \times T + 0.00034 \times GHSV - 1.27 \times Ratio - 0.000021 \times P \times GHSV - 0.088 \times P^2 - 3.91 \times 10^{-9} \times GHSV^2 - 51.51 \quad (6)$$

$$Selectivity = -11.45 \times P + 0.20 \times T + 0.0037 \times GHSV - 5.14 \times Ratio - 0.00017 \times P \times GHSV - 0.00029 \times GHSV \times Ratio + 0.41 \times P^2 - 1.86 \times 10^{-8} \times GHSV^2 + 20.77 \quad (7)$$

The high F-value of both models (Tables S5–6) implies that the models are significant and adequate to represent the actual relationship between the response and the variables [50]. The models also reveal that interactions between parameters are significant (e.g. P × GHSV and GHSV × Ratio). The predicted values of C3+ alcohol yield and selectivity match well with the experiment data (Fig. S19–20, R^2 = 0.92 for yield and R^2 = 0.91 for selectivity).

The effect of the pressure and GHSV on C3+ alcohol yield (Fig. 10) and selectivity (Fig. S21) are represented in response surface plots. It shows that intermediate pressure and GHSV are best for highest C3+ alcohol yield. This is confirmed by experiments in this regime, viz. a C3+ alcohol yield of 9.2% at 11.7 MPa, GHSV of 13500 mL g^{-1} h^{-1} (380 °C, H_2/CO ratio of 1, Table 3, entry 11). The model also predicts that a relatively high temperature and low H_2/CO ratio are also best for higher alcohol synthesis (surface plots not shown for brevity).

3.5. Comparison of catalyst performance with literature data for Mo-based catalysts

The experimentally obtained C3+ alcohol selectivity at different CO conversion over the best catalyst (K-Co-MoS_x-0.13) in this study is given in Fig. 11, together with literature data for other Mo based catalysts. Details regarding reaction conditions are shown in Table S7. Literature sources providing alcohol selectivity only on a CO_2-free basis were excluded since this leads to an overestimation of the actual C3+ alcohol selectivity and thus does not enable a fair comparison. The majority of the $KMoS_2$-based catalyst reported in the literature are promoted by Co or Ni and are supported on activated carbon (AC), carbon nanotubes (CNT), mixed metal oxides (MMO) and Al_2O_3.

It is clear that the best catalysts identified in this work (K-Co-MoS_x-0.13) outperforms all existing Mo-based catalysts. In comparison with the Co free K-MoS_2 catalyst reported previously by our groups (Table S7, entry 5), promotion with the appropriate amount of Co leads to higher selectivity and yield for C3+ alcohol.

4. Conclusions

We have prepared a series of K-Co-MoS_x catalyst with different Co contents to investigate the effect of Co promotion on product selectivity and particularly C3+ alcohol formation from syngas. The preparation of the Co-MoS_x samples through sulfurization of cobalt-molybdenum oxide precursors leads to among others the formation of Co-Mo-S and CoS_2 phases, the actual amounts being dependent on the Co amount in the catalyst formulation. The best performance was obtained using the K-Co-MoS_x-0.13 catalyst. This catalyst contains the highest amounts of Co-Mo-S and Co_9S_8 phases, implying that these are preferred for higher alcohol synthesis. It is speculated that close contact between a potassium modified Co_9S_8 phase and a Co promoted Mo-S phases is beneficial for higher alcohol synthesis due to facile transfer of adsorbed CH_x* species (and higher analogs) on the Co_9S_8 phase to oxygenated species on the Co promoted Mo-S phase to give branched higher alcohols and transfer of adsorbed $CH_3CH_2CH_2$* on the Co_9S_8 phase to adsorbed CO on the K-(Co)MoS phase to give linear alcohols. Reaction conditions (T, P, GHSV and H_2/CO ratio) were varied to study the effect on catalytic performance and models with high significance were developed. Highest C3+ alcohol yields of 7.3–9.2% and selectivities between 31.0–37.6% were obtained at a temperature of 380 °C, a pressure of 11.7 MPa, a GHSV of 13500–27000 mL g^{-1} h^{-1} and H_2/CO ratio of 1 over the optimized K-Co-MoS_x-0.13 catalyst. These results are the highest reported in the literature so far, and indicate the potential of such catalysts for further scale up studies.

Declaration of Competing Interest

The authors declare that they have no known competing financial interests or personal relationships that could have appeared to influence the work reported in this paper.

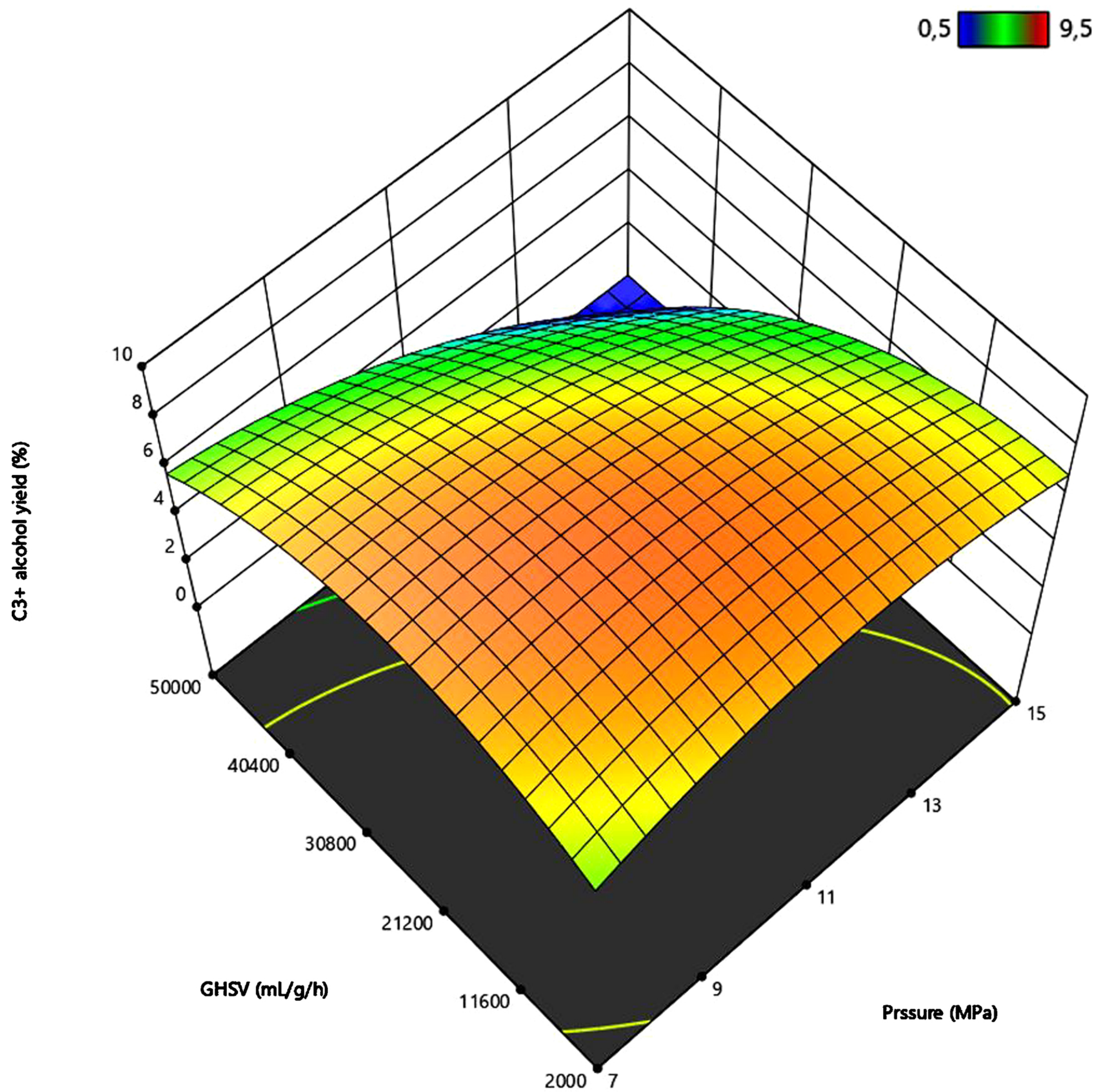

Fig. 10. Surface response plot showing the effect of GHSV and pressure on C3+ alcohol yield over the K-Co-MoS_x-0.13 catalyst (380 °C, H_2/CO molar ratio of 1).

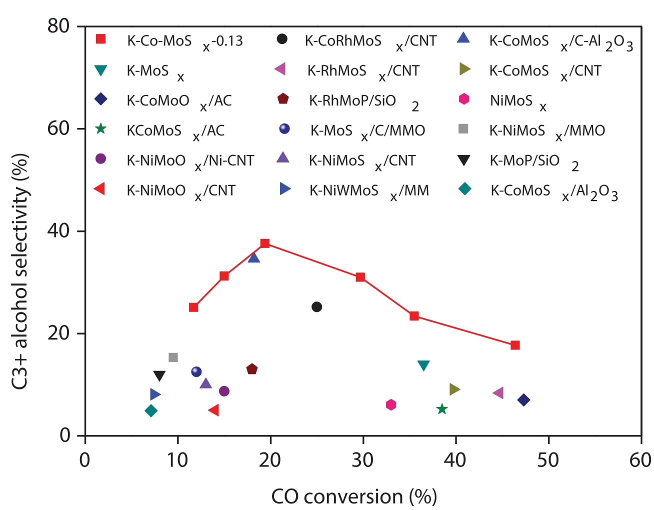

Fig. 11. Literature overview of C3+ alcohol selectivity using molybdenum-based catalysts and data for the best catalyst in this study (red squares and line).

CRediT authorship contribution statement

Xiaoying Xi: Investigation, Data curation, Formal analysis, Writing - original draft. **Feng Zeng:** Investigation, Data curation, Formal analysis, Writing - original draft. **Huatang Cao:** Investigation, Data curation, Formal analysis. **Catia Cannilla:** Investigation, Data curation, Formal analysis, Writing - review & editing. **Timo Bisswanger:** Data curation, Formal analysis, Writing - review & editing. **Sytze de Graaf:** Investigation, Data curation, Formal analysis. **Yutao Pei:** Supervision, Validation, Writing - review & editing. **Francesco Frusteri:** Supervision, Validation, Writing - review & editing. **Christoph Stampfer:** Data curation, Formal analysis. **Regina Palkovits:** Conceptualization, Supervision, Validation, Writing - review & editing. **Hero Jan Heeres:** Conceptualization, Funding acquisition, Supervision, Validation, Writing - review & editing.

Acknowledgement

Xiaoying Xi and Feng Zeng acknowledge the China Scholarship Council (CSC) for financial support.

Appendix A. Supplementary data

Supplementary material related to this article can be found, in the online version, at doi:https://doi.org/10.1016/j.apcatb.2020.118950.

References

[1] M. Balat, H. Balat, Recent trends in global production and utilization of bio-ethanol fuel, Applied energy 86 (2009) 2273–2282.
[2] T. Issariyakul, A.K. Dalai, Biodiesel from vegetable oils, Renewable and Sustainable Energy Reviews 31 (2014) 446–471.
[3] V.R. Surisetty, A.K. Dalai, J. Kozinski, Alcohols as alternative fuels: An overview, Applied Catalysis A: General 404 (2011) 1–11.
[4] E. Christensen, J. Yanowitz, M. Ratcliff, R.L. McCormick, Renewable oxygenate blending effects on gasoline properties, Energy & Fuels 25 (2011) 4723–4733.
[5] J. Li, R. Hu, H. Qu, Y. Su, N. Wang, H. Su, X. Gu, Radio-frequency thermal plasma-induced novel chainmail-like core-shell MoO_2 as highly stable catalyst for converting syngas to higher alcohols, Applied Catalysis B: Environmental 249 (2019) 63–71.
[6] H.T. Luk, C. Mondelli, D.C. Ferré, J.A. Stewart, J. Pérez-Ramírez, Status and prospects in higher alcohols synthesis from syngas, Chemical Society Reviews 46 (2017) 1358–1426.
[7] E.T. Liakakou, E. Heracleous, K.S. Triantafyllidis, A.A. Lemonidou, K-promoted NiMo catalysts supported on activated carbon for the hydrogenation reaction of CO to higher alcohols: Effect of support and active metal, Applied Catalysis B: Environmental 165 (2015) 296–305.
[8] S. Zaman, K.J. Smith, A review of molybdenum catalysts for synthesis gas conversion to alcohols: catalysts, mechanisms and kinetics, Catalysis Reviews 54 (2012) 41–132.
[9] V.P. Santos, B. van der Linden, A. Chojecki, G. Budroni, S. Corthals, H. Shibata, G.R. Meima, F. Kapteijn, M. Makkee, J. Gascon, Mechanistic insight into the synthesis of higher alcohols from syngas: the role of K promotion on MoS_2 catalysts, ACS Catalysis 3 (2013) 1634–1637.
[10] C. Liu, M. Virginie, A. Griboval-Constant, A.Y. Khodakov, Potassium promotion effects in carbon nanotube supported molybdenum sulfide catalysts for carbon monoxide hydrogenation, Catalysis Today 261 (2016) 137–145.
[11] N. Wang, R. Hu, J. Li, F. Bai, Y. Zhang, H. Su, X. Gu, Insight into the promotion mechanism of K and Ni in sulfide molybdenum-based catalysts for higher alcohols synthesis from syngas, Catalysis Communications 91 (2017) 57–61.
[12] A. Andersen, S.M. Kathmann, M.A. Lilga, K.O. Albrecht, R.T. Hallen, D. Mei, First-Principles Characterization of Potassium Intercalation in Hexagonal 2H-MoS_2, The Journal of Physical Chemistry C 116 (2012) 1826–1832.
[13] R. Andersson, M. Boutonnet, S. Järås, Correlation patterns and effect of syngas conversion level for product selectivity to alcohols and hydrocarbons over molybdenum sulfide based catalysts, Applied Catalysis A: General 417–418 (2012) 119–128.
[14] V.S. Dorokhov, D.I. Ishutenko, P.A. Nikul'shin, K.V. Kotsareva, E.A. Trusova, T.N. Bondarenko, O.L. Eliseev, A.L. Lapidus, N.N. Rozhdestvenskaya, V.M. Kogan, Conversion of synthesis gas into alcohols on supported cobalt-molybdenum sulfide catalysts promoted with potassium, Kinetics and Catalysis 54 (2013) 243–252.
[15] M. Taborga Claure, S.-H. Chai, S. Dai, K.A. Unocic, F.M. Alamgir, P.K. Agrawal, C.W. Jones, Tuning of higher alcohol selectivity and productivity in CO hydrogenation reactions over K/MoS_2 domains supported on mesoporous activated carbon and mixed MgAl oxide, Journal of Catalysis 324 (2015) 88–97.
[16] F. Zeng, X. Xi, H. Cao, Y. Pei, H.J. Heeres, R. Palkovits, Synthesis of mixed alcohols with enhanced C3+ alcohol production by CO hydrogenation over potassium promoted molybdenum sulfide, Applied Catalysis B: Environmental 246 (2019) 232–241.
[17] M. Ao, G.H. Pham, J. Sunarso, M.O. Tade, S. Liu, Active Centers of Catalysts for Higher Alcohol Synthesis from Syngas: A Review, ACS Catalysis 8 (2018) 7025–7050.
[18] V.R. Surisetty, I. Eswaramoorthi, A.K. Dalai, Comparative study of higher alcohols synthesis over alumina and activated carbon-supported alkali-modified MoS_2 catalysts promoted with group VIII metals, Fuel 96 (2012) 77–84.
[19] C. Ma, H. Li, G. Lin, H. Zhang, Ni-decorated carbon nanotube-promoted Ni–Mo–K catalyst for highly efficient synthesis of higher alcohols from syngas, Applied Catalysis B: Environmental 100 (2010) 245–253.
[20] Z. Li, Y. Fu, J. Bao, M. Jiang, T. Hu, T. Liu, Y. Xie, Effect of cobalt promoter on Co–Mo–K/C catalysts used for mixed alcohol synthesis, Applied Catalysis A: General 220 (2001) 21–30.
[21] J. Bao, Y. Fu, G. Bian, Sol–gel Preparation of K–Co–Mo Catalyst and its Application in Mixed Alcohol Synthesis from CO Hydrogenation, Catalysis Letters 121 (2008) 151–157.
[22] T. Huang, J. Xu, Y. Fan, Effects of concentration and microstructure of active phases on the selective hydrodesulfurization performance of sulfided CoMo/Al_2O_3 catalysts, Applied Catalysis B: Environmental 220 (2018) 42–56.
[23] H. Topsøe, B.S. Clausen, R. Candia, C. Wivel, S. Mørup, In situ Mössbauer emission spectroscopy studies of unsupported and supported sulfided Co-Mo hydrodesulfurization catalysts: Evidence for and nature of a Co-Mo-S phase, Journal of Catalysis 68 (1981) 433–452.
[24] G. Bian, Y. Fu, Y. Ma, Structure of Co–K–Mo/γ-Al_2O_3 catalysts and their catalytic activity for mixed alcohols synthesis, Catalysis today 51 (1999) 187–193.
[25] J. Iranmahboob, D.O. Hill, H. Toghiani, Characterization of K_2CO_3/Co–MoS_2 catalyst by XRD, XPS, SEM, and EDS, Applied surface science 185 (2001) 72–78.
[26] M. Sun, A.E. Nelson, J. Adjaye, On the incorporation of nickel and cobalt into MoS_2-edge structures, Journal of Catalysis 226 (2004) 32–40.
[27] J. Iranmahboob, D.O. Hill, H. Toghiani, K_2CO_3/Co-MoS_2/clay catalyst for synthesis of alcohol: influence of potassium and cobalt, Applied Catalysis A: General 231 (2002) 99–108.
[28] M.J. Menart, J.E. Hensley, K.E. Costelow, Thermal decomposition of bulk K-$CoMoS_x$ mixed alcohol catalyst precursors and effects on catalyst morphology and performance, Applied Catalysis A: General 437 (2012) 36–43.
[29] V.R. Surisetty, A.K. Dalai, J. Kozinski, Synthesis of higher alcohols from synthesis gas over Co-promoted alkali-modified MoS_2 catalysts supported on MWCNTs, Applied Catalysis A: General 385 (2010) 153–162.
[30] J. Iranmahboob, D.O. Hill, Alcohol Synthesis from Syngas over K_2CO_3/CoS/MoS_2 on Activated Carbon, Catalysis Letters 78 (2002) 49–55.
[31] J. Iranmahboob, H. Toghiani, D.O. Hill, Dispersion of alkali on the surface of Co-MoS_2/clay catalyst: a comparison of K and Cs as a promoter for synthesis of alcohol, Applied Catalysis A: General 247 (2003) 207–218.
[32] T. Toyoda, Y. Nishihara, E.W. Qian, CO hydrogenation on group VI metal–ceria catalysts, Fuel Processing Technology 125 (2014) 86–93.
[33] H. Li, W. Zhang, Y. Wang, M. Shui, S. Sun, J. Bao, C. Gao, Nanosheet-structured K–Co–MoS_2 catalyst for the higher alcohol synthesis from syngas: Synthesis and activation, Journal of Energy Chemistry 30 (2019) 57–62.
[34] B. Sheng, J. Liu, Z. Li, M. Wang, K. Zhu, J. Qiu, J. Wang, Effects of excess sulfur source on the formation and photocatalytic properties of flower-like MoS_2 spheres by hydrothermal synthesis, Materials Letters 144 (2015) 153–156.
[35] M.H. Siadati, G. Alonso, B. Torres, R.R. Chianelli, Open flow hot isostatic pressing assisted synthesis of unsupported MoS_2 catalysts, Applied Catalysis A: General 305 (2006) 160–168.
[36] W. Wang, K. Wu, S. Tan, Y. Yang, Hydrothermal Synthesis of Carbon-Coated CoS_2–MoS_2 Catalysts with Enhanced Hydrophobicity and Hydrodeoxygenation Activity, ACS Sustainable Chemistry & Engineering 5 (2017) 8602–8609.
[37] F. Labruyère, M. Lacroix, D. Schweich, M. Breysse, High-Pressure Temperature-Programmed Reduction of Sulfided Catalysts, Journal of Catalysis 167 (1997) 464–469.
[38] G.B. McGarvey, S. Kasztelan, An Investigation of the Reduction Behavior of MoS_2/Al_2O_3 and the Subsequent Detection of Hydrogen on the Surface, Journal of Catalysis 148 (1994) 149–156.
[39] P.J. Mangnus, A. Riezebos, A.D. Vanlangeveld, J.A. Moulijn, Temperature-Programmed Reduction and HDS Activity of Sulfided Transition Metal Catalysts: Formation of Nonstoichiometric Sulfur, Journal of Catalysis 151 (1995) 178–191.
[40] B. Yoosuk, J.H. Kim, C. Song, C. Ngamcharussrivichai, P. Prasassarakich, Highly active MoS_2, $CoMoS_2$ and $NiMoS_2$ unsupported catalysts prepared by hydrothermal synthesis for hydrodesulfurization of 4,6-dimethyldibenzothiophene, Catalysis Today 130 (2008) 14–23.
[41] B. Scheffer, N.J.J. Dekker, P.J. Mangnus, J.A. Moulijn, A temperature-programmed reduction study of sulfided Co-Mo/Al_2O_3 hydrodesulfurization catalysts, Journal of Catalysis 121 (1990) 31–46.
[42] X. Xin, Y. Song, S. Guo, Y. Zhang, B. Wang, J. Yu, X. Li, In-Situ Growth of High-Content 1T Phase MoS_2 Confined in the CuS Nanoframe for Efficient Photocatalytic Hydrogen Evolution, Applied Catalysis B: Environmental (2020) 118773.
[43] A. Müller, T. Weber, In situ raman investigation of hydrodesulphurization catalysts, Applied Catalysis 77 (1991) 243–250.
[44] K.D. Rasamani, F. Alimohammadi, Y. Sun, Interlayer-expanded MoS_2, Materials Today 20 (2017) 83–91.
[45] J. Shi, On the Synergetic Catalytic Effect in Heterogeneous Nanocomposite Catalysts, Chemical Reviews 113 (2013) 2139–2181.
[46] M. Ternan, M.J. Phillips, Proceedings 9th International Congress on Catalysis: catalysis, theory to practice, Chemical Institute of Canada, Ottawa, Ont., 1988.
[47] K.J. Smith, R.B. Anderson, A chain growth scheme for the higher alcohols synthesis, Journal of Catalysis 85 (1984) 428–436.
[48] K.J. Smith, R.G. Herman, K. Klier, Kinetic modelling of higher alcohol synthesis over alkali-promoted Cu/ZnO and MoS_2 catalysts, Chemical Engineering Science 45 (1990) 2639–2646.
[49] D. Li, C. Yang, W. Li, Y. Sun, B. Zhong, Ni/ADM: a high activity and selectivity to C_{2+}OH catalyst for catalytic conversion of synthesis gas to C_1-C_5 mixed alcohols, Topics in Catalysis 32 (2005) 233–239.
[50] P. Elavarasan, K. Kondamudi, S. Upadhyayula, Statistical optimization of process variables in batch alkylation of p-cresol with tert-butyl alcohol using ionic liquid catalyst by response surface methodology, Chemical Engineering Journal 155 (2009) 355–360.